

Electron paramagnetic resonance of tetrahedral Fe^{3+} in $\text{Bi}_4\text{Ge}_3\text{O}_{12}$ single crystals

A. Martín

Departamento de Física e Instalaciones, E.T.S. Arquitectura, Universidad Politécnica de Madrid, Avda. Juan de Herrera No. 4, E-28040 Madrid, Spain

D. Bravo, E. Diéguez, and F. J. López

Departamento de Física de Materiales C-IV, Universidad Autónoma de Madrid, Cantoblanco, E-28049 Madrid, Spain

(Received 29 February 1996; revised manuscript received 5 June 1996)

An X-band electron paramagnetic resonance study of Fe-doped $\text{Bi}_4\text{Ge}_3\text{O}_{12}$ crystals at 90 K is reported. From the angular dependence of the observed resonance lines, the spectra have been attributed to Fe^{3+} ions in the tetrahedral Ge^{4+} site. A numerical fit of the spin-Hamiltonian parameters has been carried out, giving $g_{\parallel}=2.015\pm 0.001$, $g_{\perp}=2.003\pm 0.005$, $b_2^0=-1.030\pm 0.001\text{ cm}^{-1}$, $b_4^0=(10\pm 2)\times 10^{-4}\text{ cm}^{-1}$, and $b_4^4=(-360\pm 18)\times 10^{-4}\text{ cm}^{-1}$, where the absolute signs for the b_n^m parameters are obtained from measurements at 5 K. The negative value for the “cubic” zero-field splitting parameter ($b_4^4=5a/2$) is a striking result although it can be understood within the framework of the crystal-field theory. [S0163-1829(96)03442-X]

I. INTRODUCTION

Single crystals of $\text{Bi}_4\text{Ge}_3\text{O}_{12}$ (the 2:3 stoichiometry of bismuth germanates) have found practical applications as scintillators for detection of high-energy photons and particles.¹ Also, they have attracted considerable attention owing to their potential as a solid-state laser host² and their applications in nonlinear optical devices.^{3,4} Recently, holographic gratings have been optically induced in undoped samples,⁴ as well as in samples doped with Cr (Ref. 5), Co (Ref. 6), Fe (Ref. 7) or Mn (Ref. 7).

The presence of impurities in $\text{Bi}_4\text{Ge}_3\text{O}_{12}$ (BGO) crystals is believed to play a fundamental role on these applications. On the one hand, the usefulness of BGO as a scintillator is limited by a decrease of the luminescence output induced by the photons or particles to be measured.^{8,9} Although the microscopic origin of this effect is still unclear, it has been attributed to small traces of residual impurities.^{10,11} In fact, a severe decrease of the luminescence output has been observed in crystals containing Fe, Mn, and other cationic impurities.^{12,13} It should be here remarked that iron is a particularly relevant impurity as it is commonly found in nominally pure BGO crystals.¹⁴ On the other hand, for optoelectronic applications, transition-metal-doped samples have been found to exhibit both photochromic and photorefractive effect.⁵⁻⁷ Moreover, doped samples present an enhanced photorefractive response with respect to undoped ones, the enhancement factor being about 30 for the Fe- and Mn-doped samples.⁷ Both phenomena, luminescence decrease, and enhanced photorefractive response, have been related to changes in the oxidation state of the impurities, which would act as charge traps.^{6,11} However, their electron or hole trapping character is not yet established.

In order to clarify the role of transition-metal impurities in BGO and to optimize the above-mentioned applications, a study of the position of doping ions in the host as well as their charge state is relevant. Taking into account the crystal structure of $\text{Bi}_4\text{Ge}_3\text{O}_{12}$ (see Sec. II) the metal impurities are expected to enter in a cationic site: the octahedral Bi^{3+}

and/or the tetrahedral Ge^{4+} site. It is well known that electron paramagnetic resonance (EPR) is a suitable technique for the study of magnetic impurities at low concentration levels in diamagnetic hosts. This technique has been very useful to determine the location and charge state of several $3d$ ions in BGO. So, manganese^{15,16} and cobalt¹⁷ have been detected in the Bi site as Mn^{2+} and Co^{2+} , respectively, whereas chromium has been identified both with valence $4+$ in the Ge site¹⁸ and $3+$ in the Bi site.¹⁹

However, in spite of the role that iron plays on the physical properties of BGO, no definite research on the oxidation state and structural position of this ion in BGO single crystals has been reported to date. It has however been assumed in the literature that iron occupies solely the Bi sites.¹⁴

In this work, the EPR spectrum of Fe^{3+} ions in Fe-doped BGO single crystals has been observed at RT, 90, and 5 K. From the angular dependence of the EPR spectrum at 90 K it has been ascertained, in contrast to the assumption made in the literature,¹⁴ that Fe^{3+} ions substitute for Ge^{4+} [hereafter named the Fe^{3+} (Ge) center]. Moreover, a detailed analysis of the EPR spectrum of the Fe^{3+} (Ge) center has been carried out and the parameters of the appropriate spin Hamiltonian (SH) of tetragonal symmetry have been completely determined.

From a basic point of view, the present investigation must be of interest to spectroscopists since relatively few EPR studies of Fe^{3+} in fourfold coordination exist in the literature. This is specially true for oxides, where in most cases Fe^{3+} ions appear in sixfold coordination. Even more interestingly, the SH parameters of the Fe^{3+} (Ge) center in BGO take unusually large values and the cubic zero-field splitting parameter a has been determined to be negative. Among the vast amount of EPR data for $6S$ -state ions (mainly Fe^{3+} and Mn^{2+}), negative values for a (whenever the SH is expressed in the appropriate cubic axes system) have been reported in very few cases.²⁰⁻²² Furthermore, the possible reasons for these unusual values of the SH parameters are discussed. We have found that Newman's superposition model²³ does not allow us to account satisfactorily for the SH parameters of this center. Nevertheless, it has been possible to account for the negative sign of a by means of an approach to the mi-

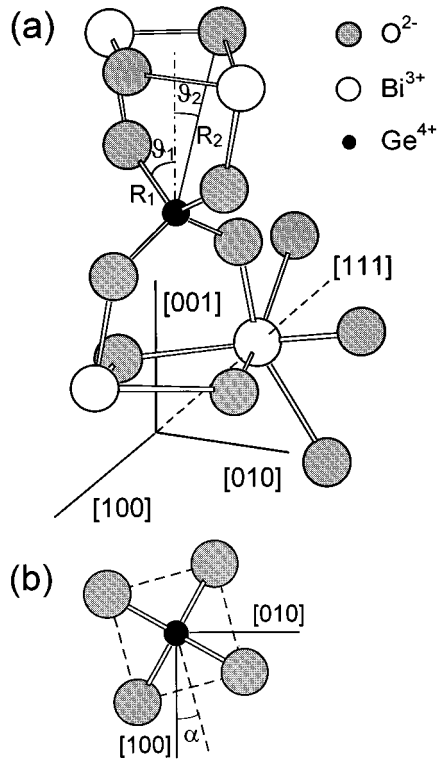


FIG. 1. (a) Partial scheme of the $\text{Bi}_4\text{Ge}_3\text{O}_{12}$ structure. The environment of Ge^{4+} is shown with the four nearest-neighbor oxygens at distance R_1 and angle θ_1 as well as the four next-nearest-neighbor oxygens with coordinates R_2 and θ_2 . The sixfold environment for one of the Bi^{3+} ions is also shown (see text). (b) Projection along the $[001]$ direction (distortion axis) of the nearest oxygen tetrahedron around Ge^{4+} showing the rotation angle α .

croscopic origin of the SH of 6S -state ions^{22,24–26} recently developed within the framework of the crystal-field (CF) theory.

II. CRYSTAL STRUCTURE AND EXPERIMENTAL METHODS

The crystal structure of $\text{Bi}_4\text{Ge}_3\text{O}_{12}$ belongs to the cubic space group $I\bar{4}3d$, with four molecules per unit cell. In this structure,^{27–29} known as eulytite, each Bi^{3+} ion is coordinated by six oxygen ions arranged in a strongly distorted octahedron with C_3 trigonal symmetry, as shown in Fig. 1(a). The threefold axis is along a $\langle 111 \rangle$ direction of the cubic cell.

Each Ge^{4+} ion (Fig. 1) is surrounded by four oxygen ions arranged in a tetrahedron slightly compressed along one of its fourfold rotary inversion axes. The distortion axis coincides with a $\langle 100 \rangle$ direction of the crystal lattice. The oxygens are located at a distance $R_1 = 1.739 \text{ \AA}$ subtending an angle $\theta_1 = 58.06^\circ$ with the distortion axis. The next-nearest neighbors of Ge are also oxygens. They are arranged in another tetrahedron strongly elongated along the same axis, with $R_2 = 3.509 \text{ \AA}$ and $\theta_2 = 23.50^\circ$. This environment yields local S_4 symmetry at the Ge^{4+} site. For each $\langle 100 \rangle$ crystal direction there are two different orientations of the Ge^{4+} site which are distinguished by a rotation $+\alpha$ or $-\alpha$ ($\alpha = 15.6^\circ$) of the nearest oxygen tetrahedron around the common distortion axis [Fig. 1(b)].

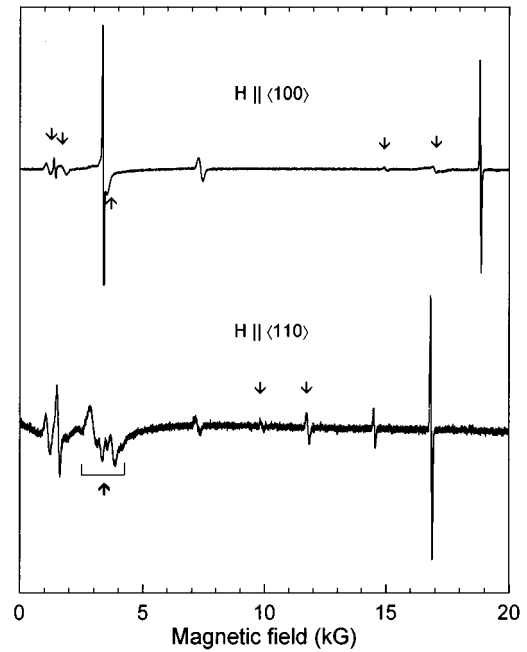


FIG. 2. EPR spectra of Fe-doped $\text{Bi}_4\text{Ge}_3\text{O}_{12}$ measured at 90 K with the magnetic field along the $\langle 100 \rangle$ and $\langle 110 \rangle$ crystal directions. Lines marked by arrows are associated to defects not studied here.

Single crystals of BGO have been grown in our laboratory by the Czochralski technique using Merck starting powders. Iron doping was achieved by adding Fe_2O_3 to the melt. The pulling direction was chosen along the $\langle 100 \rangle$ direction. Details of the growth procedure are given elsewhere.³⁰ The blocks were oriented by means of x-ray-diffraction analysis. Samples $2 \text{ mm} \times 2 \text{ mm} \times 8 \text{ mm}$ size were cut with their large faces perpendicular to $\langle 100 \rangle$ and $\langle 110 \rangle$ directions.

A Bruker ESP300 E X-band spectrometer with field modulation of 100 kHz was used to record the EPR spectra. The temperature of the sample was controlled by means of a Bruker 4121 variable temperature unit or a continuous flow liquid-helium cryostat (Oxford Instruments ESR 900) for measurements at 90 or 5 K, respectively. Accurate values of the resonance magnetic fields and microwave frequencies were measured with a nuclear magnetic resonance (NMR) gaussmeter (Bruker ER 035 M) and a frequency meter (Hewlett-Packard 5342A), respectively. The crystals were mounted on a rotating sample holder for measurements of the angular variation of the EPR spectra.

III. EXPERIMENTAL RESULTS AND IMPURITY LOCATION

The EPR spectrum of Fe-doped BGO samples, can be detected from room temperature down to 5 K. Figure 2 shows the EPR spectra recorded at 90 K, with the magnetic field \mathbf{H} directed along $\langle 100 \rangle$ and $\langle 110 \rangle$ directions. For these special orientations, several lines collapse giving rise to a spectrum simpler than for an arbitrary orientation. The first derivative lines have peak-to-peak linewidths ranging from 50 to 170 G at 90 K. No hyperfine structure was observed even at 5 K. Lines corresponding to various defects were detected, although a complete study of the angular variation has been carried out only for the more intense lines which

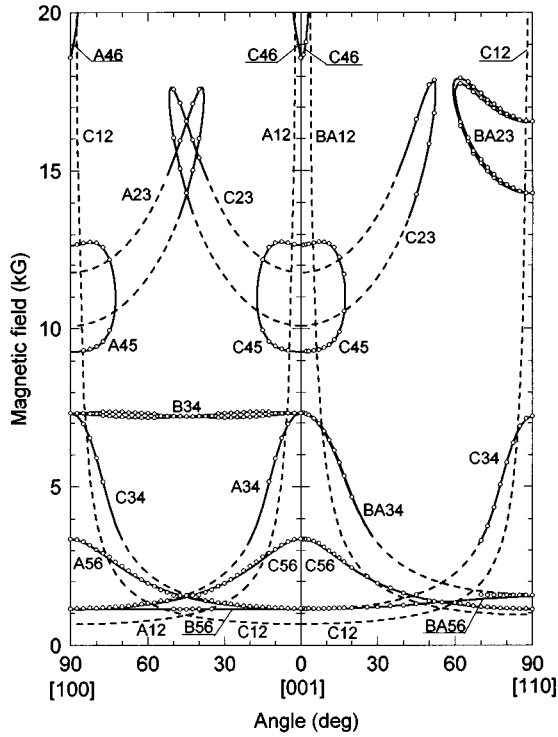


FIG. 3. Angular variation of the EPR spectrum at 90 K with \mathbf{H} lying in planes $\{100\}$ and $\{110\}$. Open circles show the experimental resonance positions, while the calculated ones are plotted with lines. Continuous (dashed) lines correspond to transitions of high (low) probability. Resonances arising from centers with the Z axis along $[100]$, $[010]$, and $[001]$ directions are labeled A, B, and C, respectively. Transitions are labeled with the numbers of the two levels involved. Numbers 1 to 6 correspond to states $| -5/2 \rangle$, $| +5/2 \rangle$, . . . , $| +1/2 \rangle$, respectively, in the low-field limit.

correspond to the center described here. The angular variation of the EPR spectrum for that center has been measured at 90 K for \mathbf{H} lying in $\{100\}$ and $\{110\}$ planes. The experimental resonance fields have been plotted with open circles in Fig. 3. The observed strong angular dependence as well as the presence of loops for some lines reveal a high-spin system with a large zero-field splitting. These features, the absence of hyperfine structure and the fact that the spectrum is detected even at room temperature indicate that it is due to Fe^{3+} ions ($3d^5$, $6S_{5/2}$).

The angular dependence of the spectrum agrees with a defect having axial symmetry along the $\langle 100 \rangle$ crystal directions. As only the Ge^{4+} site has the distortion axis along these directions (S_4 symmetry), we are led to propose that Fe^{3+} substitutes for Ge^{4+} ions [$\text{Fe}^{3+}(\text{Ge})$ center]. This result is somewhat surprising since Fe^{3+} would be expected to substitute for Bi^{3+} , as they have the same charge state. In fact, it has been assumed in the literature¹⁴ that Fe^{3+} enters the Bi^{3+} site. Moreover, this is the site occupied by all EPR-studied trivalent impurities reported to date in $\text{Bi}_4\text{Ge}_3\text{O}_{12}$ doped with Gd, Er, Nd, and Cr (Refs. 31–33, 19). However, Fe^{3+} has been found by EPR to substitute for Ge^{4+} in $\text{Bi}_{12}\text{GeO}_{20}$,³⁴ and for Si^{4+} in $\text{Bi}_{12}\text{SiO}_{20}$.³⁵

The resonance line positions depend on the magnetic-field orientation (θ , φ) with respect to the defect principal axes (X, Y, Z). The Z axis is chosen along the $\langle 100 \rangle$ fourfold sym-

metry axis, whereas X and Y are rotated an angle α' with respect to the crystallographic $\langle 100 \rangle$ axes. It should be remarked that the angle α' is expected to be close to the rotation angle α of the first-neighbor oxygen tetrahedron [Fig. 1(b)] because these ions are the main responsible for the crystal field at the impurity site. The $\text{Fe}^{3+}(\text{Ge})$ model gives rise to six magnetically nonequivalent centers for an arbitrary magnetic-field orientation as consequence of the six different orientations of the Ge site in the unit cell (see Sec. II). This allows us to explain the angular variation of the lines (Fig. 3) in the following way. When the magnetic field is along the $[001]$ direction, we observe the spectra for two groups of centers. On the one side, there is a set of two centers with their distortion axis Z along that direction ($\theta=0^\circ$), having X and Y axes rotated by angles α' and $-\alpha'$ around Z , respectively (denoted C in Fig. 3). On the other side, the two sets which have their Z axis along $[100]$ and $[010]$ directions (denoted A and B, respectively) are perpendicular to the magnetic field ($\theta=90^\circ$). Each center belonging to set A or B has its X and Y axes rotated an angle $+\alpha'$ or $-\alpha'$ around the common Z axis. Thus, for $\mathbf{H} \parallel [001]$, defects with $\pm\alpha'$ are equivalent and only two groups of lines (parallel and perpendicular) are observed in the spectrum. However, when the magnetic field is rotated in the (010) plane towards the $[100]$ direction, the four perpendicular centers are no longer equivalent. Two of them (set B, with $Z \parallel [010]$) remain perpendicular to \mathbf{H} , but are magnetically nonequivalent as the φ angle takes a different value because α' has different sign. This gives rise to the observed small splitting in the lines around 7300 G in Fig. 3. This α' splitting is also observed in Fig. 3 for lines labeled BA23 near 14 300 and 16 500 G when $\mathbf{H} \parallel [110]$.

IV. ANALYSIS OF THE EPR SPECTRUM

The appropriate spin Hamiltonian to analyze the EPR spectrum of a Fe^{3+} ion ($S=5/2$), occupying a cubic site axially distorted along a tetragonal axis (local symmetries D_4 , C_{4v} , D_{2d} , D_{4h} , C_4 , S_4 or C_{4h}) is³⁶

$$\hat{\mathcal{H}} = g_{\parallel} \beta H_Z \hat{S}_Z + g_{\perp} \beta (H_X \hat{S}_X + H_Y \hat{S}_Y) + \frac{1}{3} b_2^0 \hat{O}_2^0 + \frac{1}{60} (b_4^0 \hat{O}_4^0 + b_4^4 \hat{O}_4^4), \quad (1)$$

where the first two terms account for the Zeeman interaction. The fine structure is expressed by means of Stevens operator equivalents \hat{O}_n^m .³⁷ The b_n^m are parameters to be determined from experiment and are commonly named fine structure or zero-field splitting (ZFS) parameters. The axes of the coordinate system for the spin Hamiltonian are chosen coincident with the X, Y, Z axes of each defect. With this choice the $b_4^{-4} \hat{O}_4^{-4}$ term in the spin Hamiltonian vanishes.^{36,38}

The value for g_{\parallel} can be accurately obtained from the expression for the $+1/2 \leftrightarrow -1/2$ transition³⁷ (near 3300 G) when \mathbf{H} is directed along one tetragonal $\langle 100 \rangle$ axis. In this case the resonance field is $H_{\text{res}} = h\nu/g_{\parallel}\beta$, thus giving $g_{\parallel} = 2.015$.

As shown by Geschwind,³⁹ the angle α' can be directly obtained from the position of the turning points in the angular variation of the lines corresponding to the two defects

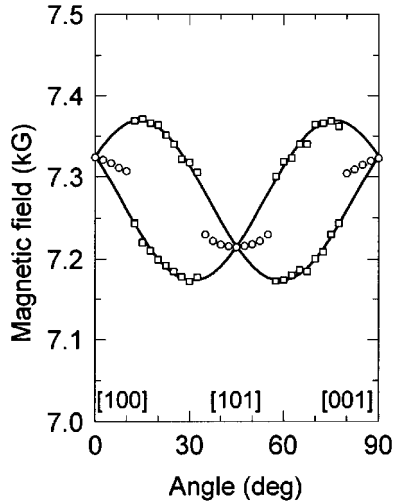


FIG. 4. Detailed view of the line B34 in the $\{100\}$ angular variation of Fig. 3. Experimental resonance fields have been decomposed into two lines (open squares) corresponding to defects which remain perpendicular to \mathbf{H} and are rotated angles α' and $-\alpha'$. Open circles stand for experimental results where the decomposition could not be carried out reliably. Continuous lines show the calculated resonance fields with the parameters given in Table I.

whose Z axis remains perpendicular to the magnetic field. This is our case for the lines showing a small splitting near 7300 G when the magnetic field lies in a $\{100\}$ plane (labeled B34 in Fig. 3), although for many orientations these lines appear unresolved. A decomposition of these lines has been carried out by a deconvolution method and the results are shown in Figs. 3 and 4. In this way, a first estimation yields $\alpha' \approx 15^\circ$ or 30° , each choice giving opposite sign for b_4^4 . However, as in the BGO structure $\alpha = 15.6^\circ$ we choose the first value for α' , which would indicate that the defect principal axes are scarcely rotated around the Z axis with respect to the GeO_4^{4-} tetrahedron in the perfect lattice.

From those initial values for g_{\parallel} and α' the fitting of the SH parameters to the angular-variation data was carried out by numerical diagonalization of the energy matrix expressed in the $|S, M_S\rangle$ basis, where $S = 5/2$. The values to fit are the experimental line positions corresponding to defects whose Z axis forms 0° , 45° and 90° with the magnetic field, as well as the splitting between the lines corresponding to the two defects at angles $\pm\alpha'$ [lines B34 in (010) and BA23 in (110) planes in Fig. 3]. A grid method was used to obtain the best-fit values for the SH parameters. If an isotropic g matrix

is assumed, a misfit appears between calculated and measured values for $\theta = 90^\circ$. This could only be avoided considering an anisotropic g matrix, as reported for Fe^{3+} in some few cases.^{40,41} The best fit is obtained for $\alpha' = 14 \pm 1^\circ$ and the parameters given in Table I. The resonance fields calculated with these parameters are represented as continuous and dashed lines in Figs. 3 and 4, which show the good agreement obtained between the experimental and predicted resonance fields. This result ensures the validity of the above spin Hamiltonian and confirms the proposed location of Fe at the Ge site. Moreover it indicates that the iron center maintains the S_4 symmetry of the Ge site.

It is interesting to point out the fact that the resonance fields for transition B34 in Fig. 4 are higher for the magnetic field along the $\langle 100 \rangle$ than along the $\langle 110 \rangle$ directions. In the calculations this can only be achieved by taking the same relative sign for the ZFS parameters b_2^0 and b_4^4 in the chosen system (XYZ). On the other hand, it must be noted that the fitting provides only absolute values for the parameters together with the relative signs of the b_n^m parameters. In order to obtain the absolute signs of these parameters (given in Table I), we have carried out measurements at 5 K. After considering the energy-level scheme, the absolute sign of the zero-field splitting parameters was determined from the relative intensities of transitions at 300 and 5 K, and b_2^0 was found to be negative.

The zero-field splitting is usually described by means of the parameters D , a , and F . Their values in the present case are also included in Table I because the discussion in the next section will also be carried out in terms of these parameters. The parameters for other defects of Fe^{3+} tetrahedrally coordinated by oxygen in several hosts have been included in the table for the sake of comparison.

V. DISCUSSION

First, we point out the striking values for the obtained SH parameters as compared with those for tetrahedrally coordinated Fe^{3+} in other compounds (see Table I). In particular, the parameters D , F , and a take unusually large values, which are unexpected if one considers the nearly regular arrangement of the four oxygens around the Ge site (see Sec. II). A very remarkable feature is the negative sign for a . To our knowledge, all the previously reported values of a for tetrahedrally coordinated Fe^{3+} are positive if one takes the (XYZ) reference system as in this work. In what follows, possible reasons for these unusual values will be discussed.

TABLE I. Best-fit values of the SH parameters for Fe^{3+} in $\text{Bi}_4\text{Ge}_3\text{O}_{12}$ at 90 K. The ZFS parameters (in units of 10^{-4} cm^{-1}) are expressed in two commonly used notations. The relation between the two notations is $D = b_2^0$, $a = \frac{2}{5}b_4^4$, $F = 3b_4^0 - \frac{3}{5}b_4^4$. Values for other defects of Fe^{3+} tetrahedrally coordinated by oxygen in several hosts are also included. Parentheses indicate errors in the last digits.

Material	g_{\parallel}	g_{\perp}	$b_2^0 = D$	b_4^0	b_4^4	F	a	α' (deg)	α (deg)	Reference
$\text{Bi}_4\text{Ge}_3\text{O}_{12}$	2.015(1)	2.003(5)	-10300 (10)	10 (2)	-360(18)	247 (16)	-144(7)	14 (1)	15.6	This work
$\text{Bi}_{12}\text{GeO}_{20}$	2.003(2)	2.003(2)	0	24.5	122.5	0	49(5)	0	0	34
$\text{Y}_3\text{Ga}_5\text{O}_{12}$	2.0047(5)	2.0047(5)	-880(6)	18	155	-38(5)	62(4)	16.5	15.8	39
$\text{Lu}_3\text{Ga}_5\text{O}_{12}$	2.003(1)	2.003(1)	-1131(5)	17	163	-47(5)	65(5)	16	15.2	42
$\text{Y}_3\text{Al}_5\text{O}_{12}$	2.004(1)	2.004(1)	-1028(5)	1	188	-110(5)	75(5)	16	17.9	42
$\text{Lu}_3\text{Al}_5\text{O}_{12}$	2.004(1)	2.004(1)	-1249(5)	7	210	-104(5)	84(5)	16.5	16.5	42

A. Charge compensation

The large values for the ZFS parameters could be related to local charge compensation. In fact, charge compensation must occur due to the substitution of Fe^{3+} for Ge^{4+} . This can be reasonably achieved by oxygen vacancies V_o . A first-neighbor oxygen vacancy would account for the large value of the parameter D (or b_2^0), which is comparable to those measured for $\text{Fe}^{3+}\text{-}V_o$ centers in perovskites.⁴³ However, this cannot happen in our case since one of the defect axes should then point along the iron-vacancy direction which disagrees with the determined defect axes. Charge compensation could also result from some cationic mechanism. For example, Bi^{5+} substituting for the tetravalent cation as proposed for $\text{Bi}_{12}\text{SiO}_{20}\text{:Fe}^{3+}$.³⁵ However, this should not produce an important effect at the impurity site because the nearest Ge^{4+} site along the Z axis is far away (10.513 Å). Alternatively, a monovalent cation at an interstitial position would compensate the charge and could account for the large D value if it is close to iron along the Z axis. However, this possibility can also be ruled out because it would lower the local symmetry of the center from S_4 to C_2 and then additional terms would be required in the spin Hamiltonian to fit the spectra. Therefore, we conclude that charge compensation must be nonlocal in any case. This implies that the values for the ZFS parameters result primarily from the arrangement of the oxygen ions around iron.

B. Superposition model analysis of ZFS parameters

Information about the local environment of impurity ions is frequently obtained by means of Newman's superposition model (SM).²³ This model was originally proposed to express the parameters B_{nm} of the crystal-field (CF) as a sum of independent axial contributions coming from the nearest-neighbor ions (usually named ligands). In the model, each parameter B_{nm} is written as

$$B_{nm} = \sum_i \bar{B}_n(R_0) \left(\frac{R_0}{R_i} \right)^{T_n} K_{nm}(\theta_i, \varphi_i), \quad (2)$$

where R_i , θ_i , φ_i are the polar coordinates of ligand i referred to the central ion in the defect axes system, and $K_{nm}(\theta_i, \varphi_i)$ are the coordination factors. $\bar{B}_n(R_0)$ are intrinsic parameters giving the contribution to the crystal field for a specific ligand at distance R_0 and T_n express the potential dependence of this contribution in the neighborhood of R_0 .

The model was later extended to analyze the ZFS parameters b_n^m of 6S -state ions and it has been used to obtain information about the crystalline local environment of such ions. The expressions for these b_n^m parameters are formally identical to Eq. (2) but the values of the intrinsic parameters $\bar{b}_n(R_0)$ and exponents t_n are very different from those appropriate to the B_{nm} parameters (typically $t_2 \sim 8$, $t_4 \sim 14$ for $3d^5$ ions with oxygen ligands).

We have attempted to analyze our ZFS parameters with the SM in order to explain their values and to estimate the lattice relaxation of the first oxygen shell around the impurity. First of all, a direct estimation of the relaxed angle θ_1 (Fig. 1) can be made from the experimental value of the ratio b_4^0/b_4^4 . This is because, in the case of S_4 or D_{2d} symmetries,

the expression for this ratio given by the SM depends neither on the intrinsic parameters nor on the distances R_1 . In our defect axes system, we obtain

$$\frac{b_4^0}{b_4^4} = \frac{35 \cos^4 \theta_1 - 30 \cos^2 \theta_1 + 3}{-35 \sin^4 \theta_1}. \quad (3)$$

This equation gives two solutions for θ_1 which in our case are either ≈ 30 or 70° . This is to say, that the SM expressions for the fourth-order parameters point to very strong relaxations of the oxygen tetrahedron, either elongated or compressed, which are difficult to believe. It is to be noted that Eq. (3) also gives unreasonable values of θ_1 for tetrahedrally coordinated Fe^{3+} in garnets.

Now, the second-order parameter b_2^0 is analyzed with the appropriate SM expression:

$$b_2^0 = 2\bar{b}_2(R_0) \left(\frac{R_0}{R_1} \right)^{t_2} (3 \cos^2 \theta_1 - 1). \quad (4)$$

To this end, assuming the lattice values for R_1 (1.739 Å), we have first used the set of intrinsic parameters ($\bar{b}_2 = -0.2058 \text{ cm}^{-1}$ for $R_0 = 1.8 \text{ Å}$ and $t_2 = 6$) obtained from tetrahedrally coordinated Fe^{3+} in garnets,²⁴ which seem adequate to our case. However, this set gives the unreasonable result $\theta_1 \approx 0^\circ$. Then we have tried the commonly used values $\bar{b}_2 = -0.412 \text{ cm}^{-1}$ at $R_0 = 2.101 \text{ Å}$ and $t_2 = 8$ given by Siegel and Müller⁴⁴ for octahedrally coordinated Fe^{3+} . The calculation yields $\theta_1 \approx 49^\circ$, which is a reasonable value, although it implies a strong relaxation (elongation) from the lattice value (58.06°) and is very far from the values for θ_1 derived from the fourth-order parameters.

C. Crystal-field theory analysis of ZFS parameters

In view of the inconsistent results provided by the superposition model, we have attempted to explain the sign and value of the ZFS parameters within the framework of a crystal-field approach in which the ZFS parameters arise as a consequence of the combined effect of the crystal-field and spin-orbit interactions. The dependence of the ZFS parameters b_n^m on the CF parameters B_{nm} has been recently elucidated for a $3d^5$ ion by Yu and Rudowicz.²⁶ These authors found that each b_n^m parameter depends on all B_{nm} parameters. The ‘‘cubic’’ ZFS parameter a has two contributions $a = a_c + a_t$. The component a_c comes from the cubic crystal field Dq and is always positive. Whereas a_t , the contribution due to the low-symmetry field components (tetragonal in this case), depends on B_{20} and Dq similarly to F . The a_t contribution for tetrahedral Fe^{3+} in garnets²⁵ has been found to be positive and as large as the a_c contribution, explaining satisfactorily the magnitude and positive sign for a in those crystals.

In order to explain the negative sign of our experimental a value, the a_t contribution should in this case be negative and larger than a_c . We can estimate a_t from our experimental F value taking into account that the crystal-field theory predicts the ratio a_t/F to be nearly insensitive to all CF parameters and to range from -0.2 to -0.5 for usual values of the CF parameters.²⁶ From our experimental F value, the cited range predicts a_t values between -50 and $-123 \times 10^{-4} \text{ cm}^{-1}$. If we take for a_c the value obtained from the purely

cubic spectrum of tetrahedral Fe^{3+} in $\text{Bi}_{12}\text{GeO}_{20}$ ($a_c \equiv a = 49 \times 10^{-4} \text{ cm}^{-1}$),³⁴ we obtain values for a between -1 and $-74 \times 10^{-4} \text{ cm}^{-1}$. It is to say, the crystal-field theory allows us to explain the negative sign of a . The experimental ratio a_c/F would be $a_c/F = (a - a_c)/F = -0.78 \pm 0.08$, using the a_c value cited above. The fact that this ratio lies outside the predicted range may be due to unusually large values of the CF parameters, expected also from the large values obtained for D and F . Also, one must bear in mind that the CF theory does not consider the role of covalency overlap and relativistic effects. Moreover, for tetrahedral environments it

has been pointed out the importance of odd-parity field components which mix the ground configuration $3d^5$ with the excited configurations of odd parity.²² It follows that more theoretical work is needed to fully explain our experimental data.

ACKNOWLEDGMENT

This work was partially supported by the Spanish Comisión Interministerial de Ciencia y Tecnología (CICYT) under Project No. PB94-0147-C02.

- ¹B. G. Grabmaier, IEEE Trans. Nucl. Sci. **NS-31**, 372 (1984).
- ²A. A. Kaminskii, S. E. Sarkisov, G. A. Denisenko, V. V. Ryabchenkov, V. A. Lomonov, Yu E. Perlin, M. G. Blazha, D. Schultze, B. Hermoneit, and P. Reiche, Phys. Status Solidi **A 85**, 553 (1984).
- ³S. K. Kurz and T. T. Perry, J. Appl. Phys. **39**, 3798 (1968).
- ⁴G. Montemezzani, St. Pfändler, and P. Günter, J. Opt. Soc. Am. **B 9**, 1110 (1992).
- ⁵E. Moya, L. Contreras, and C. Zaldo, J. Opt. Soc. Am. **B 5**, 1737 (1988).
- ⁶C. Zaldo and E. Diéguez, Opt. Mater. **1**, 171 (1992).
- ⁷C. Zaldo, E. Moya, L. F. Magaña, L. Kovács, and K. Polgár, J. Appl. Phys. **73**, 2114 (1993).
- ⁸G. J. Bobbink, A. Engler, R. W. Kraemer, J. Nash, and R. B. Sutton, Nucl. Instrum. Methods Phys. Res. Sect. A **227**, 470 (1984).
- ⁹C. Laviron and P. Lecoq, Nucl. Instrum. Methods Phys. Res. Sect. A **227**, 45 (1984).
- ¹⁰C. Zaldo and E. Moya, J. Phys. Condens. Matter **5**, 4935 (1993).
- ¹¹L. Kovács, E. Moya, K. Polgar, F. J. López, and C. Zaldo, Appl. Phys. A **52**, 307 (1991).
- ¹²He Chongfan, Fan Shiji, Liao Jingying, Shen Quanshun, Shen Dingzhong, and Zhou Tiangun, Progr. Crystal Growth Charact. **11**, 253 (1985).
- ¹³T. Q. Zhou, H. R. Tan, C. F. He, R. Y. Zhu, and H. B. Newman, Nucl. Instrum. Methods Phys. Res. Sect. A **258**, 58 (1987).
- ¹⁴R. G. L. Barnes, J. Cryst. Growth **69**, 248 (1984).
- ¹⁵D. Bravo, L. Arizmendi, M. Aguilar, and F. J. López, J. Phys. Condens. Matter **2**, 10 123 (1990).
- ¹⁶D. Bravo and F. J. López, J. Phys. Condens. Matter **3**, 7691 (1991).
- ¹⁷D. Bravo, A. Martín, and F. J. López, Solid State Commun. **86**, 281 (1993).
- ¹⁸F. J. López, E. Moya, and C. Zaldo, Solid State Commun. **76**, 1169 (1990).
- ¹⁹D. Bravo and F. J. López, Solid State Commun. **85**, 415 (1993).
- ²⁰J. Rubio O. and W. K. Cory, J. Chem. Phys. **69**, 4792 (1978).
- ²¹J. C. Hensel, Bull. Am. Phys. Soc. **9**, 244 (1964).
- ²²Wan-Lun Yu, Phys. Rev. **B 39**, 622 (1989).
- ²³D. J. Newman and Betty Ng, Rep. Prog. Phys. **52**, 699 (1989).
- ²⁴Wan-Lun Yu and Min-Guang Zhao, Phys. Rev. **B 37**, 9254 (1988).
- ²⁵Wan-Lun Yu, Phys. Rev. **B 41**, 9415 (1990).
- ²⁶Wan-Lun Yu and Czeslaw Rudowicz, Phys. Rev. **B 45**, 9736 (1992).
- ²⁷G. Menzer, Z. Kristallogr. **78**, 136 (1931).
- ²⁸A. A. Kaminskii, D. Schultze, B. Hermoneit, S. E. Sarkisov, L. Li, J. Bohm, P. Reiche, R. Ehlert, A. A. Mayer, V. A. Lomonov, and V. A. Balashov, Phys. Status Solidi **A 33**, 737 (1976).
- ²⁹D. J. Segal, R. P. Santoro, and R. E. Newnham, Z. Kristallogr. **123**, 73 (1966).
- ³⁰M. T. Santos, J. C. Rojo, L. Arizmendi, and E. Diéguez, J. Cryst. Growth **142**, 103 (1994).
- ³¹B. Blanzat, F. Raynal, R. Parrot, C. Barthou, and B. Canny, Phys. Status Solidi **B 76**, K5 (1976).
- ³²D. Bravo and F. J. López, J. Chem. Phys. **99**, 4952 (1993).
- ³³D. Bravo, A. Martín, A. A. Kaminskii, and F. J. López, Radiat. Eff. Defects Solids **135**, 191 (1995).
- ³⁴W. Wardzyński, M. Baran, and H. Szymczak, Physica **111B**, 47 (1981).
- ³⁵H. J. von Bardeleben, J. Phys. **D 16**, 29 (1983).
- ³⁶D. G. McGavin, J. Magn. Reson. **74**, 19 (1987).
- ³⁷A. Abragam and B. Bleaney, *Electron Paramagnetic Resonance of Transition Ions* (Dover, New York, 1986), p. 437.
- ³⁸Czeslaw Rudowicz, Magn. Reson. Rev. **13**, 1 (1987).
- ³⁹S. Geschwind, Phys. Rev. **121**, 363 (1961).
- ⁴⁰Hyunsoo So and Michael T. Pope, J. Chem. Phys. **55**, 2786 (1971).
- ⁴¹E. López Carranza and R. T. Cox, J. Phys. Chem. Solids **40**, 413 (1979).
- ⁴²L. Rimai and T. Kushida, Phys. Rev. **143**, 160 (1966).
- ⁴³E. Siegel, W. Urban, K. A. Müller, and E. Wiesendangen, Phys. Lett. **A 53**, 415 (1975).
- ⁴⁴E. Siegel and K. A. Müller, Phys. Rev. **B 20**, 3587 (1979).